Class. Quantum Grav. **22** (2005) 4253–4261 doi:10.1088/0264-9381/22/20/007

Optimal time-domain combination of the two calibrated output quadratures of GEO 600

M Hewitson[1], H Grote[1], S Hild[1], H Lück[1], P Ajith[1], J R Smith[1], K A Strain[2], B Willke[1] and G Woan[2]

[1] Max-Planck-Institut für Gravitationsphysik (Albert-Einstein-Institut) und Universität Hannover, Außenstelle Hannover, Callinstr. 38, 30167 Hannover, Germany
[2] Physics and Astronomy, University of Glasgow, Glasgow G12 8QQ, Great Britain

E-mail: martin.hewitson@aei.mpg.de

Received 8 July 2005, in final form 18 August 2005
Published 27 September 2005
Online at stacks.iop.org/CQG/22/4253

Abstract

GEO 600 is an interferometric gravitational wave detector with a 600 m arm-length and which uses a dual-recycled optical configuration to give enhanced sensitivity over certain frequencies in the detection band. Due to the dual-recycling, GEO 600 has two main output signals, both of which potentially contain gravitational wave signals. These two outputs are calibrated to strain using a time-domain method. In order to simplify the analysis of the GEO 600 data set, it is desirable to combine these two calibrated outputs to form a single strain signal that has optimal signal-to-noise ratio across the detection band. This paper describes a time-domain method for doing this combination. The method presented is similar to one developed for optimally combining the outputs of two colocated gravitational wave detectors. In the scheme presented in this paper, some simplifications are made to allow its implementation using time-domain methods.

PACS numbers: 95.55.Br, 95.75.Kk, 04.80.Nn, 95.55.Ym

1. Introduction

GEO 600 [1] is part of an international network of gravitational wave observatories which is searching for gravitational wave signatures from various source types. GEO 600 is the only long-baseline dual-recycled Michelson interferometer in the world. With its 600 m arm-length, it should, when fully commissioned, be sensitive to strain amplitudes of the order of $1 \times 10^{-22}\ \mathrm{Hz}^{-1/2}$.

GEO 600 uses a dual-recycling configuration which means that two additional mirrors are added to the standard Michelson interferometer optical layout. One mirror, the power-recycling (PR) mirror, is added at the input port of the Michelson. Since the Michelson interferometer in GEO 600 is operated at a dark fringe, the light reflected from the input port is made resonant by the cavity formed between the PR mirror and the Michelson. Another mirror, the signal-recycling (SR) mirror, is placed at the output of the Michelson to create a resonant cavity for any signal sidebands that leave the interferometer (see [2, 3] for details).

The use of signal recycling gives an enhancement in strain sensitivity over a certain band of frequencies. This band is defined by the reflectivity of the SR mirror and the length of the SR cavity. One consequence of using such an optical scheme is that the gravitational wave (GW) signal gained from demodulating the detector output at the frequency of the control sidebands is spread between the two demodulation quadratures. This means that, for a given demodulation phase, the GW signal content in one quadrature can only be optimized for one frequency; at all other frequencies, the demodulation phase is not optimal. In the absence of noise, the complete signal could be recovered by calibrating only one of the output quadratures. However, since there is noise in the system, the data from both output quadratures need to be calibrated such that at any given frequency, the data stream with the best signal-to-noise ratio is available for analysis. Having calibrated both output data streams, we have two estimates for the detected strain of the interferometer. This is somewhat undesirable since a choice must be made, based on the analysis to be performed, as to which strain signal to analyse.

To remove the need for this choice, we seek to combine the two calibrated output signals of GEO 600 into a single strain signal that has an optimal signal-to-noise ratio at all frequencies in the detection band (40 Hz–6 kHz). In addition, as we will see, the combination of the two calibrated streams, if done correctly, leads to a signal that is more sensitive than either of the two separate signals. In order to fit in with the current calibration scheme of GEO 600, we want to do this combination in the time domain.

2. Time-domain calibration of GEO 600

The calibration of GEO 600 is done using a time-domain method. Calibration lines are continuously injected into the differential length-control actuators of the Michelson interferometer at a few frequencies across the detection band. The response of the detector to this differential displacement, and hence to strain, is computed once per second by forming the transfer function from the injection point to the two detector outputs; a model of this transfer function is then fit to the measurements. This model is then inverted and used to create time-domain filters. By filtering the two detector outputs, $P(t)$ and $Q(t)$, through these time-domain filters, we recover two estimates, $h_{\mathrm{P}}(t)$ and $h_{\mathrm{Q}}(t)$, of the apparent detected strain of the interferometer. The details, development and application of the calibration scheme are given in [4–8]. The method runs in real time with a latency of a few seconds.

3. Optimal combination of two calibrated output signals of GEO 600

The combination of the two calibrated output signals of GEO 600 can be done by considering the variance of the noise in the two signals in a particular frequency bin. Here we wish to combine the two signals together so as to achieve the best estimate of the detected gravitational wave strain. In addition, we want to take into account any correlations that may exist between the two calibrated output signals.

3.1. Maximum likelihood method of combining two signals

We start from the assumption that the two calibrated output signals, h_{P} and h_{Q}, contain the same gravitational wave signals. This is true to a level consistent with the accuracy of the calibration of each output signal. In addition, each calibrated output contains noise components which will, in general, be different, but may be correlated to a varying degree at some frequencies. Then we can write

$$h_{\mathrm{P}}(t) = h(t) + N_{\mathrm{P}}(t), \tag{1}$$

$$h_{\mathrm{Q}}(t) = h(t) + N_{\mathrm{Q}}(t), \tag{2}$$

where $h(t)$ is the underlying signal we seek, and $N_{\mathrm{P}}(t)$ and $N_{\mathrm{Q}}(t)$ represent the noise in the two calibrated output quadratures.

The method centres around the covariance matrix of the two signals:

$$\mathrm{C} = \begin{pmatrix} \sigma_{\mathrm{PP}} & \sigma_{\mathrm{PQ}} \\ \sigma_{\mathrm{QP}} & \sigma_{\mathrm{QQ}} \end{pmatrix},$$

where $\sigma_{\mathrm{QP}} = \langle \tilde{N}_{\mathrm{P}} \tilde{N}_{\mathrm{Q}}^{*} \rangle = \sigma_{\mathrm{PQ}}^{*}$, and $\tilde{}$ denotes the Fourier transform. Here, the cross terms σ_{PQ} and σ_{QP} are the variances of those signal components that are common to both h_{P} and h_{Q}. These terms are, in general, complex functions of frequency.

For a single frequency, f, it can be shown that the optimal combination of the two calibrated strain signals is given by

$$\hat{h}(f) = \frac{h_{\mathrm{P}}(f)\sigma_{\mathrm{QQ}}(f) + h_{\mathrm{Q}}(f)\sigma_{\mathrm{PP}}(f) - \sigma_{\mathrm{PQ}}(f)h_{\mathrm{P}}(f) - \sigma_{\mathrm{QP}}h_{\mathrm{Q}}(f)}{\sigma_{\mathrm{PP}}(f) + \sigma_{\mathrm{QQ}}(f) - [\sigma_{\mathrm{PQ}}(f) + \sigma_{\mathrm{QP}}(f)]}, \tag{3}$$

where $\hat{h}(f)$ is a maximum likelihood estimate for the underlying gravitational wave strain signature, $h(f)$. An outline of the derivation of equation (3) is given in the appendix. (This expression for $\hat{h}(f)$ can also be derived using a minimum variance method, see the appendix of [9] for details.)

3.2. Computing the weighting functions

In order to apply the formula given in equation (3) in the time domain, we must compute the optimal combination for each frequency in the detection band, and convert this array of 'weights' into time-domain filters.

The variance terms, σ_{PP} and σ_{QQ}, in equation (3) can be estimated by looking at the noise components of the two calibrated signals at each frequency; in other words, by considering the noise floor of the power spectral density (PSD) of each signal. (The variance of a particular signal at a given frequency is proportional to the mean value of the PSD at that frequency.) How good an estimate this is depends on the observation time and stationarity of the signal when making the PSD. If the noise is stationary, then the estimate of the PSD, and hence of the variance, can be improved by taking more and more averages. If the noise is non-stationary, then the PSD needs to be constructed over the appropriate time scale. The noise in the GEO 600 output is sufficiently stationary on time scales of many hours, and so the assumption is fine for all practical purposes.

The terms σ_{PQ} and σ_{QP} can be estimated for each frequency by considering the noise floor of the cross-power spectral density of h_{P} and h_{Q}; the same considerations of stationarity and observation time apply as for the diagonal terms. In addition, we assume that the means of the two data streams at a given frequency are zero; this is a good approximation over the frequency range we are dealing with since we have removed any coherent signals when making the noise-floor estimation.

Figure 1 shows typical power spectral density estimates of h_{P} and h_{Q}, together with an estimate of the cross-power spectral density (CSD); a noise-floor estimate for each is also shown. The phase components of the CSD are shown in figure 2. The noise-floor estimates

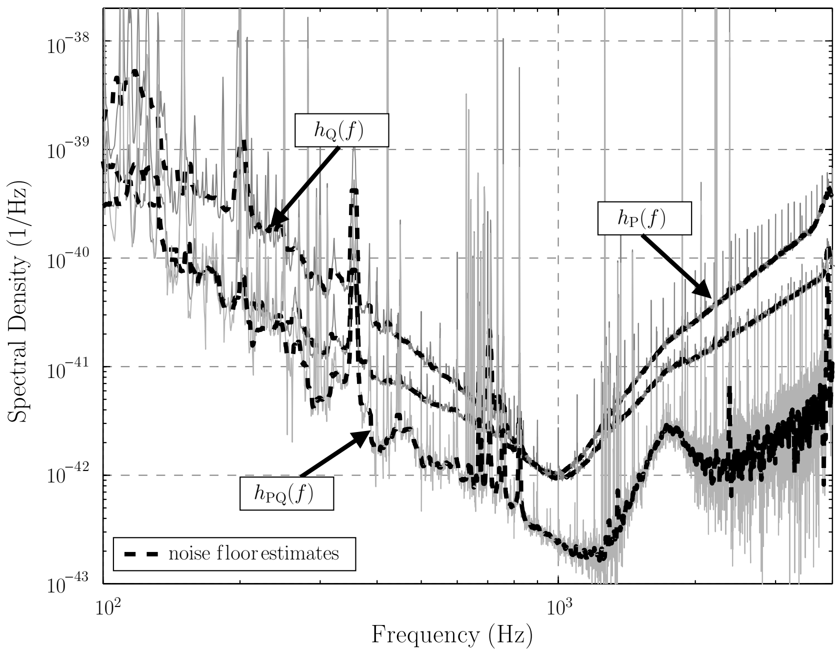

Figure 1. Power- and cross-spectral densities of the two calibrated outputs of GEO 600 (light coloured curves). Noise-floor estimates constructed from a running median estimator are also shown (dark coloured curves). The frequency axis is cut off at 100 Hz to limit the dynamic range of the displayed data; the calibration and the combining procedure are valid down to 50 Hz.

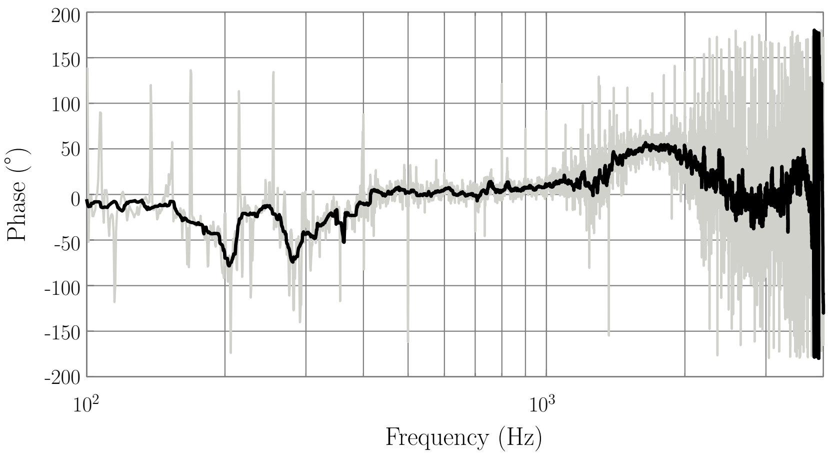

Figure 2. The phase components of the cross-spectral density of $h_P(t)$ and $h_Q(t)$. A 'noise-floor estimate' is also shown.

are constructed by using a running median estimator. For a particular frequency bin, f, the values in the surrounding N bins are sorted in ascending order and the top h_{cut}% are discarded in order to discard outliers (from lines, for example). The median of the remaining values is taken as an estimate of the noise floor at the frequency f. For the noise-floor estimates shown in figure 1, $N = 32$ bins and $h_{cut} = 0.9$.

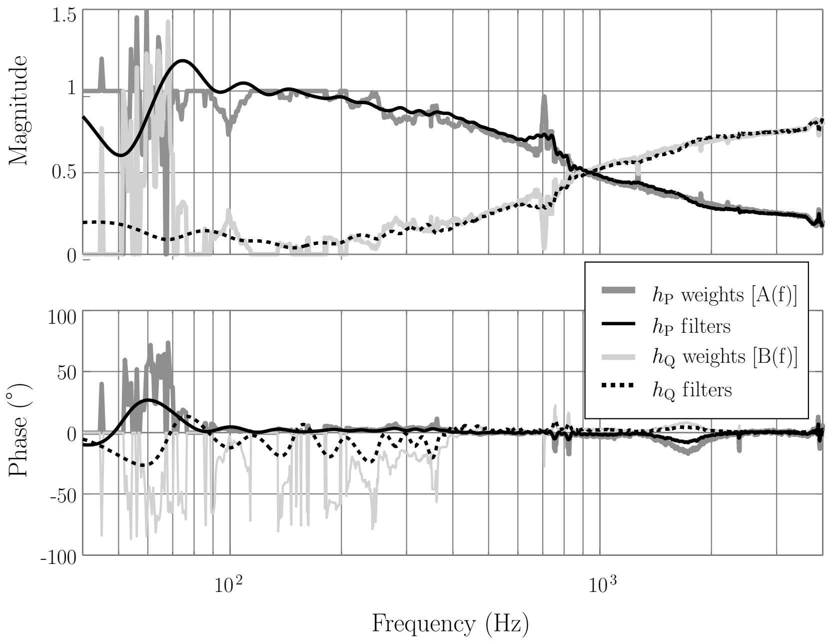

Figure 3. The optimal weighting functions for combining signals $h_P(f)$ and $h_Q(f)$ which have the power- and cross-spectral densities shown in figure 1. Also shown are the overall magnitude and phase responses of the filter pairs designed using the method described in the text.

Equation (3) can be re-written such that we have two complex frequency-dependent weighting factors, $A(f)$ and $B(f)$, for h_P and h_Q:

$$\hat{h}(f) = A(f)h_P(f) + B(f)h_Q(f), \tag{4}$$

where

$$A(f) = \frac{\sigma_{QQ}(f) - \sigma_{PQ}(f)}{\sigma_{PP}(f) + \sigma_{QQ}(f) - [\sigma_{PQ}(f) + \sigma_{QP}(f)]}, \tag{5}$$

$$B(f) = \frac{\sigma_{PP}(f) - \sigma_{QP}(f)}{\sigma_{PP}(f) + \sigma_{QQ}(f) - [\sigma_{PQ}(f) + \sigma_{QP}(f)]}. \tag{6}$$

Figure 3 shows an example of the magnitude and phase of the weighting functions for the data used in figures 1 and 2.

3.3. Designing the filters

The weighting functions that were computed in the previous section are, in general, complex. In order to make time-domain filter representations of these two weighting functions, we need a way to compute time-domain filters that have arbitrary magnitude and phase responses. One such method is to consider the magnitude and phase responses separately. We can write $A(f)$ and $B(f)$ in terms of their magnitude and phase parts such that

$$A(f) = a(f)\,e^{i\phi_a(f)}, \tag{7}$$

$$B(f) = b(f)\,e^{i\phi_b(f)}. \tag{8}$$

Now we construct four filters, $\mathcal{M}_P$, $\mathcal{P}_P$, $\mathcal{M}_Q$ and $\mathcal{P}_Q$ which have the frequency responses, $a(f)$, $e^{i\phi_a(f)}$, $b(f)$ and $e^{i\phi_b(f)}$, respectively.

Construction of the time-domain filters, $\mathcal{M}_{\rm P}$ and $\mathcal{M}_{\rm Q}$, is done by assuming that the response we seek ($a(f)$ and $b(f)$) are the Fourier transforms of the impulse responses of the two linear-phase time-domain filters [10–12]. For this to be the case, we need to generate the appropriate phase delay for the two filters. This is just a frequency-dependent linear-phase shift defined by the filter order we require. If we want filters of order $N_{\rm taps}$, then we construct a grid of $N_{\rm G}$ equally spaced frequency points that run from 0 to the Nyquist rate and estimate the magnitude and phase at each point. The magnitude estimates come directly from $a(f)$ and $b(f)$ (interpolated or averaged as necessary), and the phase components are just linear with frequency starting from 0 phase shift, such that

$$\tilde{\mathcal{M}}_{\rm P}(f) = a(j)\exp\left[\frac{-(N_{\rm taps}-1){\rm i}\pi j}{2(N_{\rm G}-1)}\right], \tag{9}$$

$$\tilde{\mathcal{M}}_{\rm Q}(f) = b(j)\exp\left[\frac{-(N_{\rm taps}-1){\rm i}\pi j}{2(N_{\rm G}-1)}\right], \tag{10}$$

where $\tilde{\mathcal{M}}_{\rm P}(f)$ denotes the response of the filter $\mathcal{M}_{\rm P}$ (the single-sided Fourier transform of the impulse response), ${\rm i} = \sqrt{-1}$, and $j \in [0 : N_{\rm G})$.

We can then form the two-sided Fourier transform of the impulse response of the filter by concatenating the vector $\tilde{\mathcal{M}}_{\rm P}(f)$ with the reverse sequence of the conjugate of $\tilde{\mathcal{M}}_{\rm P}(f)$; the same is done for $\tilde{\mathcal{M}}_{\rm Q}(f)$. Thus we have a frequency series that runs from $-f_{\rm s}/2$ to $+f_{\rm s}/2$. This is what we would get from the Fourier transform of a real data series. If we take the inverse transform, and apply a window function, we get the filter coefficients we seek for $\mathcal{M}_{\rm P}$ and $\mathcal{M}_{\rm Q}$. The time shifts introduced when applying these filters can simply be removed by appropriate buffering of the filtered signals.

The filters representing the phase components of the weighting functions are constructed as all-pass filters. Here the magnitude response of the filter is designed to be unity for a significant part of the pass-band. The phase response is an approximation to that phase response we seek. These filters can be designed by minimizing the difference between the desired response, ${\rm e}^{{\rm i}\phi_a(f)}$, and the response of the filter, $\tilde{\mathcal{P}}_{\rm P}(f)$ using, for example, a nonlinear least-squares routine. The error-function that was minimized in this application was

$$\epsilon = \Sigma_k |\tilde{\mathcal{P}}_{\rm P}(f_k) - {\rm e}^{{\rm i}\phi_a(f_k)}|^2. \tag{11}$$

An example of the combined magnitude and phase response of $\mathcal{M}_{\rm P}$ with $\mathcal{P}_{\rm P}$, and $\mathcal{M}_{\rm Q}$ with $\mathcal{P}_{\rm Q}$ is shown in figure 3. Also shown are the original weighting functions. (The linear-phase response of $\mathcal{M}_{\rm P}$ and $\mathcal{M}_{\rm Q}$ is omitted for clarity). The examples shown are 300 tap filters for the magnitude parts, and 512 tap filters for the phase parts.

3.4. Results

Having constructed the time-domain filters, we can easily compute the optimal $h(t)$ signal in the time-domain by

$$h(t) = \tilde{\mathcal{M}}_{\rm P}\{h_{\rm P}(t)\} + \tilde{\mathcal{P}}_{\rm P}\{h_{\rm P}(t)\} + \tilde{\mathcal{M}}_{\rm Q}\{h_{\rm Q}(t)\} + \tilde{\mathcal{P}}_{\rm Q}\{h_{\rm Q}(t)\}. \tag{12}$$

The result of applying this to real GEO 600 data is shown in figure 4. Here we see three amplitude spectral densities constructed from $h_{\rm P}(t)$, $h_{\rm Q}(t)$ and $h(t)$.

An amplitude spectral density of the injected calibration signal calibrated to strain is also shown. The calibration peaks used for determining the detector response are indicated with filled markers. In order to confirm that the constructed time-domain filters are performing properly, we can look at a relative comparison of the calibrated and combined strain signals to the induced strain signal. By computing the magnitude and phase of the calibration peaks in

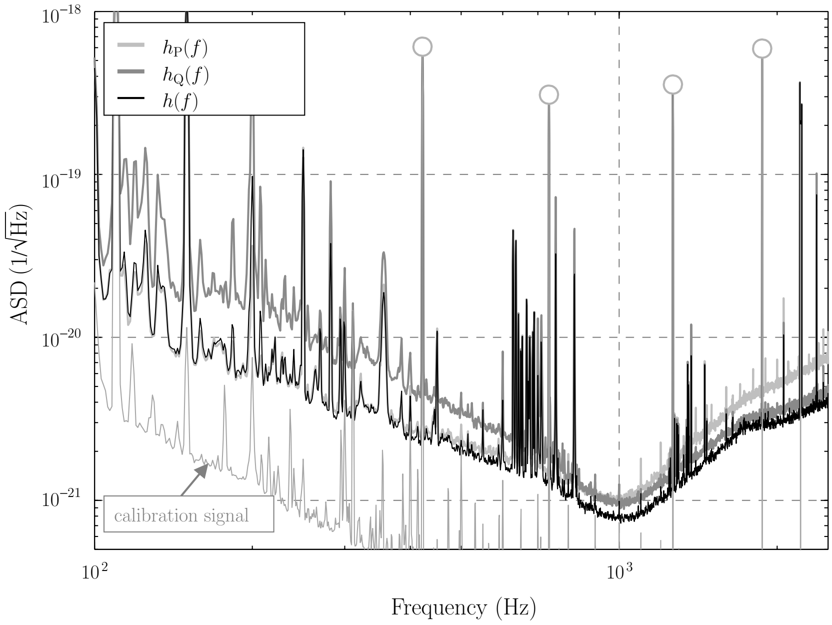

Figure 4. Snap-shot amplitude spectral densities (ASD) of the two calibrated outputs of GEO 600, $h_P(t)$, $h_Q(t)$ and of the optimally combined signal $h(t)$. Injected calibration lines are highlighted with filled markers. An ASD of the strain induced by the injected calibration signal is also shown with the peaks marked by the grey circles. The frequency axis is cut off at 100 Hz to limit the dynamic range of the displayed data; the calibration and the combining procedure are valid down to 50 Hz.

all signals, we can form the magnitude ratio and phase difference between the induced strain, and the three computed strain signals. Figure 5 shows the results of this calculation for the data stretch shown in figure 4. We can see that, at least at these spot-frequencies, the combined $h(t)$ preserves the signal present in the underlying $h_P(t)$ and $h_Q(t)$ to a good degree. (The apparent inaccuracy of the $Q(t)$ output calibration at 110 Hz comes from the measurement of the calibration line at this frequency due to the presence of other spectral features, and not from inaccuracies in the calibration process.)

4. Summary and future work

The on-line calibration scheme used at GEO 600 was extended to include an optimal time-domain combination of the two calibrated output signals. The result is a single $h(t)$ signal that is at least as sensitive as either of the two calibrated output signals at all frequencies in the detection band, and is a significant improvement at some frequencies. One further step is to allow for time-variation in the optimal combination filters. This means determining the filters on-line periodically, and then smoothly moving from using one set of filters to the next. This is in principle straightforward, with the complexity lying only in the implementation since we wish to maintain the real-time, low-latency nature of the current system. In addition, the combining filters shown in this paper have a much smoother response than the underlying weighting functions. This is due to the difficulties in making the phase correction filters with very high numbers of taps. Using a more sophisticated optimisation routine may be one way

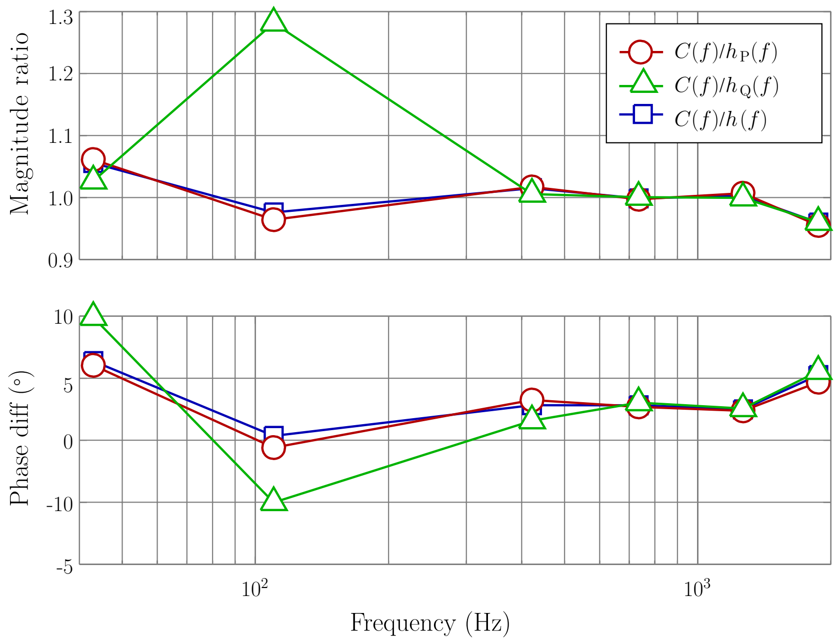

Figure 5. The magnitude ratio and phase difference of the strain induced by injecting calibration lines to the detected strain as measured in the two calibrated output signals, as well as the combined strain signal. The comparison is made at each calibration line frequency.

to produce more detailed combining filters; this remains to be investigated and developed further.

Acknowledgments

The authors would like to thank Albert Lazzarini and Joe Romano for their help and discussions regarding the methods presented in [9].

Appendix. Maximum likelihood estimator for $h(t)$

We are given two pieces of data, h_p and h_q, which are generally complex and are related to a complex parameter h by

$$h_\mathrm{p} = h + N_\mathrm{p} \tag{A.1}$$

$$h_\mathrm{q} = h + N_\mathrm{q}. \tag{A.2}$$

We write this in vector form as

$$\mathbf{d} = \mathbf{h} + \mathbf{N}. \tag{A.3}$$

The noises are complex and correlated with a (Hermitian) covariance matrix

$$\mathrm{C} = \begin{pmatrix} \sigma_\mathrm{pp} & \sigma_\mathrm{pq} \\ \sigma_\mathrm{qp} & \sigma_\mathrm{qq} \end{pmatrix}, \tag{A.4}$$

where

$$\sigma_{ij} = \langle N_i N_j^* \rangle \tag{A.5}$$

and * denotes the complex conjugate. The determinant of this matrix is

$$\det \mathrm{C} = \sigma_{\mathrm{pp}}\sigma_{\mathrm{qq}} - \sigma_{\mathrm{qp}}\sigma_{\mathrm{pq}} = \sigma_{\mathrm{pp}}\sigma_{\mathrm{qq}} - |\sigma_{\mathrm{pq}}|^2 \tag{A.6}$$

and its inverse is

$$\mathrm{C}^{-1} = \frac{1}{\det \mathrm{C}} \begin{pmatrix} \sigma_{\mathrm{qq}} & -\sigma_{\mathrm{pq}} \\ -\sigma_{\mathrm{qp}} & \sigma_{\mathrm{pp}} \end{pmatrix}. \tag{A.7}$$

The likelihood of h is the probability of the given data h, taken to be a complex bivariate Gaussian, i.e.,

$$p(h_{\mathrm{p}}, h_{\mathrm{q}}|h) = \frac{1}{\pi^2 \det \mathrm{C}} \exp[-(\mathbf{d} - \mathbf{h})^{\mathrm{H}} \mathrm{C}^{-1} (\mathbf{d} - \mathbf{h})], \tag{A.8}$$

with $\mathbf{x}^{\mathrm{H}}$ being the conjugate transpose of $\mathbf{x}$. The maximum likelihood estimator for h is the value that maximizes this probability, or alternatively minimizes

$$Q = (\mathbf{d} - \mathbf{h})^{\mathrm{H}} \mathrm{C}^{-1} (\mathbf{d} - \mathbf{h}) \tag{A.9}$$

$$= \mathbf{d}^{\mathrm{H}} \mathrm{C}^{-1} \mathbf{d} + \mathbf{h}^{\mathrm{H}} \mathrm{C}^{-1} \mathbf{h} - 2\,\mathrm{Re}\{\mathbf{h}^{\mathrm{H}} \mathrm{C}^{-1} \mathbf{d}\} \tag{A.10}$$

with respect to the real and imaginary components of h. Our constraints are therefore

$$\frac{\partial Q}{\partial\, \mathrm{Re}\{h\}} = 0, \qquad \frac{\partial Q}{\partial\, \mathrm{Im}\{h\}} = 0. \tag{A.11}$$

Multiplying out individual terms we get

$$\mathbf{h}^{\mathrm{H}} \mathrm{C}^{-1} \mathbf{h} = \frac{hh^*}{\det \mathrm{C}} (\sigma_{\mathrm{pp}} + \sigma_{\mathrm{qq}} - \sigma_{\mathrm{pq}} - \sigma_{\mathrm{qp}}) \tag{A.12}$$

and

$$\mathbf{h}^{\mathrm{H}} \mathrm{C}^{-1} \mathbf{d} = \frac{h^*}{\det \mathrm{C}} [h_{\mathrm{p}}(\sigma_{\mathrm{qq}} - \sigma_{\mathrm{pq}}) + h_{\mathrm{q}}(\sigma_{\mathrm{pp}} - \sigma_{\mathrm{qp}})], \tag{A.13}$$

so the maximum likelihood estimator of h is

$$\hat{h}_{\mathrm{ML}} = \frac{h_{\mathrm{p}}(\sigma_{\mathrm{qq}} - \sigma_{\mathrm{pq}}) + h_{\mathrm{q}}(\sigma_{\mathrm{pp}} - \sigma_{\mathrm{qp}})}{(\sigma_{\mathrm{pp}} + \sigma_{\mathrm{qq}}) - (\sigma_{\mathrm{pq}} + \sigma_{\mathrm{qp}})}. \tag{A.14}$$

Note the denominator of this is purely real.

References

[1] Smith J R *et al* 2004 Commissioning, characterization, and operation of the dual-recycled GEO 600 *Class. Quantum Grav.* **21** S1737–45

[2] Heinzel G *et al* 2002 Dual recycling for GEO 600 *Class. Quantum Grav.* **19** 1547–53

[3] Grote H, Freise A, Malec M, Heinzel G, Willke B, Lück H, Strain K A, Hough J and Danzmann K 2004 Dual recycling for GEO 600 *Class. Quantum Grav.* **21** S473–80

[4] Hewitson M, Grote H, Heinzel G, Strain K A, Ward H and Weiland U 2003 Calibration of the power-recycled gravitational wave detector, GEO 600 *Rev. Sci. Instrum.* **74** 4184

[5] Hewitson M, Grote H, Heinzel G, Strain K A, Ward H and Weiland U 2003 Calibration of GEO 600 for the S1 science run *Class. Quantum Grav.* **20** S885–93

[6] Hewitson M, Heinzel G, Smith J R, Strain K A and Ward H 2004 Principles of calibrating the dual-recycled GEO 600 *Rev. Sci. Instrum.* **75** 4702

[7] Hewitson M *et al* 2004 Calibration of the dual-recycled GEO 600 detector for the S3 science run *Class. Quantum Grav.* **21** S1711–22

[8] Hewitson M (for the LIGO Scientific Collaboration) 2005 Preparing GEO 600 for gravitational astronomy—a status report *Class. Quantum Grav.* **22** S891–900

[9] Lazzarini A *et al* 2004 Optimal combination of signals from colocated gravitational wave interferometers for use in searches for a stochastic background *Phys. Rev.* D **70** 062001

[10] Mitra S K 1998 *Digital Signal Processing A Computer Based Approach* 1st edn (New York: McGraw-Hill) pp 462–68

[11] Jackson L B 1996 *Digital Filters and Signal Processing* 3rd edn (Boston, MA: Kluwer) pp 301–7

[12] Oppenheim A V and Shafer R W 1999 *Discrete-Time Signal Processing* 2nd edn *(Prentice Hall Signal Processing Series)* (Englewood Cliffs, NJ: Prentice-Hall)